



Kedar, S., Andrade, J., Banerdt, B., Delage, P., Golombek, M., Grott, M., Hudson, T., Kiely, A., Knapmeyer, M., Knapmeyer-Endrun, B., Krause, C., Kawamura, T., Lognonne, P., Pike, T., Ruan, Y., Spohn, T., Teanby, N., Tromp, J., & Wookey, J. (2017). Analysis of regolith properties using seismic signals generated by InSight's HP3 Penetrator. *Space Science Reviews*. <https://doi.org/10.1007/s11214-017-0391-3>

Peer reviewed version

Link to published version (if available):  
[10.1007/s11214-017-0391-3](https://doi.org/10.1007/s11214-017-0391-3)

[Link to publication record in Explore Bristol Research](#)  
PDF-document

This is the author accepted manuscript (AAM). The final published version (version of record) is available online via Springer at <https://link.springer.com/article/10.1007%2Fs11214-017-0391-3>. Please refer to any applicable terms of use of the publisher.

## University of Bristol - Explore Bristol Research

### General rights

This document is made available in accordance with publisher policies. Please cite only the published version using the reference above. Full terms of use are available:  
<http://www.bristol.ac.uk/red/research-policy/pure/user-guides/ebr-terms/>

# **Analysis of regolith properties using seismic signals generated by InSight's HP<sup>3</sup> penetrator**

Sharon Kedar<sup>1</sup>, Jose Andrade<sup>2</sup>, Bruce Banerdt<sup>1</sup>, Pierre Delage<sup>3</sup>, Matt Golombek<sup>1</sup>,  
Matthias Grott<sup>4</sup>, Troy Hudson<sup>1</sup>, Aaron Kiely<sup>1</sup>, Martin Knapmeyer<sup>4</sup>, Brigitte  
Knapmeyer-Endrun<sup>5</sup>, Christian Krause<sup>6</sup>, Taichi Kawamura<sup>7</sup>, Philippe Lognonne<sup>7</sup>,  
Tom Pike<sup>8</sup>, Youyi Ruan<sup>9</sup>, Tilman Spohn<sup>4</sup>, Nick Teanby<sup>10</sup>, Jeroen Tromp<sup>9</sup>, James  
Wookey<sup>10</sup>

<sup>1</sup>Jet Propulsion Laboratory, California Institute of Technology, Pasadena, California, USA  
Sharon.Kedar@jpl.nasa.gov

<sup>2</sup>Department of Mechanical and Civil Engineering, , California Institute of Technology,  
Pasadena, California, USA

<sup>3</sup>Ecole des Ponts ParisTech, Navier-CERMES, France

<sup>4</sup>Deutsches Zentrum für Luft- und Raumfahrt e.V. (DLR), Berlin Germany

<sup>5</sup>Max Planck Institute for Solar System Research, Göttingen, Germany

<sup>6</sup>DLR, Köln, Germany

<sup>7</sup>Institut de Physique du Globe de Paris, Paris, France

<sup>8</sup>Imperial College of London, London, UK

<sup>9</sup>Princeton University, Princeton, New Jersey, USA

<sup>10</sup>School of Earth Sciences, University of Bristol, Bristol, UK

## 1. Abstract

InSight's Seismic Experiment for Interior Structure (SEIS) provides a unique and unprecedented opportunity to conduct the first geotechnical survey of the Martian soil by taking advantage of the repeated seismic signals that will be generated by the mole of the Heat Flow and Physical Properties Package (HP<sup>3</sup>). Knowledge of the elastic properties of the Martian regolith have implications to material strength and can constrain models of water content, and provide context to geological processes and history that have acted on the landing site in western Elysium Planitia. Moreover, it will help to reduce travel-time errors introduced into the analysis of seismic data due to poor knowledge of the shallow subsurface. The challenge faced by the InSight team is to overcome the limited temporal resolution of the sharp hammer signals, which have significantly higher frequency content than the SEIS 100 Hz sampling rate. Fortunately, since the mole propagates at a rate of ~1mm per stroke down to 5m depth, we anticipate thousands of seismic signals, which will vary very gradually as the mole travels.

Using a combination of field measurements and modeling we simulate a seismic data set that mimics the InSight HP<sup>3</sup>-SEIS scenario, and the resolution of the InSight seismometer data. We demonstrate that the direct signal, and more importantly an anticipated reflected signal from the interface between the bottom of the regolith layer and an underlying lava flow, are likely to be observed both by InSight's Very Broad Band (VBB) seismometer and Short Period (SP) seismometer. We have outlined several strategies to increase the signal temporal resolution using the multitude of hammer stroke and internal timing information to stack and interpolate multiple signals, and demonstrated that in spite of the low resolution, the key parameters –seismic velocities and regolith depth – can be retrieved with a high degree of confidence.

## 1 Introduction

The InSight (Interior Exploration using Seismic Investigations, Geodesy and Heat Transport) mission will be the first Mars lander to place an ultra-sensitive broadband seismometer on the planet's surface. About a meter away from the seismometer, a Heat Flow and Physical Properties Package (HP<sup>3</sup>) experiment will hammer a probe 5 m into the Martian subsurface to measure the heat coming from Mars' interior and reveal the planet's thermal history (Figure 1). The probe, which uses a self-hammering mechanism, will generate thousands of seismic signals that can be used to analyze the shallow (several tens of meters) subsurface and shed new light on the mechanical properties of the Martian regolith. The descent will progress in ~0.5 m hammering intervals, each interval taking between 0.5–4 hours, and each interval being separated by several days of thermal measurements. Each hammering interval consists of several hundred to several thousand strokes ~3 s apart, depending on the regolith properties.

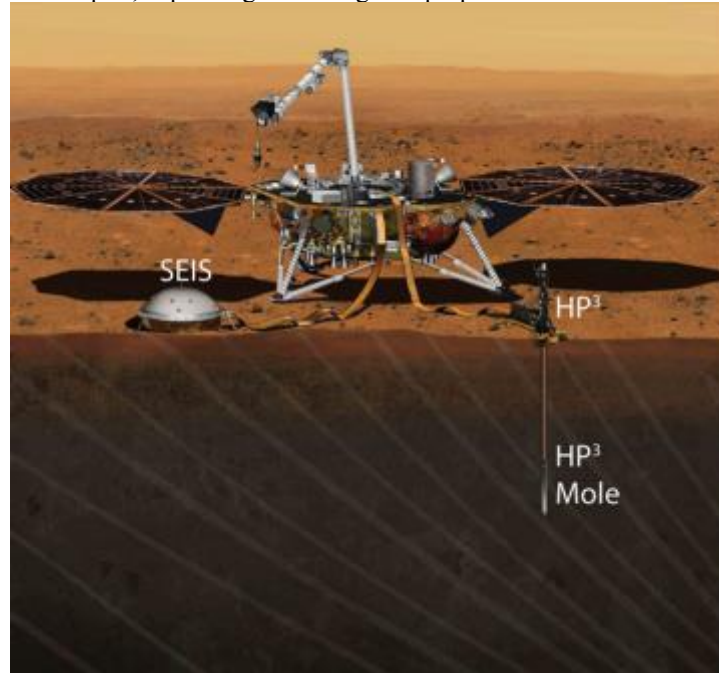


Figure 1: An illustration of the InSight lander in its final configuration on the Martian surface. A Very Broad-band triaxial seismometer is deployed ~1-2 m away from heat probe with a self-hammering mole that will gradually penetrate down to 5 m below the surface.

Although not included in the mission's level 1 science objectives, which focus on planetary-scale seismic and tectonic processes and their implications to rocky planet formation, the proximity of a repeating hammer source to a sensitive seismometer presents a unique opportunity to study the shallow geological structure at the landing site. Understanding the seismic properties of Martian regolith and determining its thickness will certainly reduce InSight's seismic measurement errors. However, an added benefit is the opportunity to conduct the first ever seismic geotechnical study of the Martian soil and provide new essential knowledge for future robotic and human exploration missions.

Given that geotechnical analysis of the landing site was not part of the mission threshold objectives, InSight's Seismic Experiment for Interior Structure (SEIS) was not designed to accommodate the high sampling rates and strict source-sensor timing synchronization requirements that are part and parcel of similar terrestrial surveys. Nevertheless, the seismometer's sensitivity and the multitude of hammering impulses make near-surface seismic exploration of Mars feasible.

In this paper we outline the methodologies that will be incorporated in the analysis of HP<sup>3</sup>'s seismic signals to overcome some of the technical challenges that SEIS operation presents.

Through a combination of laboratory measurements and numerical simulations we demonstrate that we will be able to determine the seismic pressure and shear (P and S) wave velocity, the thickness of the regolith layer and the corresponding mechanical properties of the regolith.

## 2. Experimental Set-Up

### 2.1 InSight Landing Site: Geologic Setting, Physical Properties and Subsurface Structure

InSight will land in western Elysium Planitia on Hesperian plains just north of the dichotomy boundary [Golombek *et al.*, this issue]. This location satisfies the three dominant landing site engineering constraints, which are latitude ( $3^{\circ}\text{N}$ - $5^{\circ}\text{N}$ ), elevation ( $<-2.5$  km with respect to the MOLA geoid), and a large smooth, flat surface to place a 130 km by 27 km landing ellipse. Other engineering constraints that are relevant to the geologic setting include: 1) a load bearing, radar reflective surface with thermal inertia  $>100$  to  $140 \text{ J m}^{-2} \text{ K}^{-1} \text{ s}^{-1/2}$ , slopes  $<15^{\circ}$  and rock abundance  $<10\%$  for safe landing and instrument deployment, and a broken up regolith  $>5$  m thick for full penetration of the HP<sup>3</sup> mole [Golombek *et al.*, 2013a, this issue].

The InSight landing ellipse is located on smooth plains with Noachian highlands to the south and west, a ridge of Medusae Fossae Formation to the southeast and very young lavas from Athabasca Valles to the east. The ellipse is located at  $4.5^{\circ}\text{N}$ ,  $136.1^{\circ}\text{E}$  about 540 km north of the Curiosity landing site. The plains surface on which the InSight ellipse is located is mapped as Early Hesperian transition unit (eHt) by Tanaka *et al.* [2014] in the global geologic map of Mars, which could be sedimentary or volcanic. A volcanic interpretation of the plains is supported by: 1) the presence of rocks in the ejecta of fresh craters  $\sim 0.15$ -20 km diameter arguing for a strong competent layer  $\sim 10$ -200 m deep [e.g., Golombek *et al.*, 2013b, this issue; Catling *et al.*, 2011, 2012], 2) exposures of strong, jointed bedrock overlain by  $\sim 10$  m of fine grained regolith in nearby Hephaestus Fossae in southern Utopia Planitia at  $21.9^{\circ}\text{N}$ ,  $122.0^{\circ}\text{E}$  [Golombek *et al.*, 2013b], 3) platy and smooth lava flows mapped in 6 m/pixel visible images south of the landing site [Ansan *et al.*, 2015], and 4) the presence of wrinkle ridges, which have been interpreted to be fault-propagation folds, in which slip on thrust faults at depth is accommodated by asymmetric folding in strong, but weakly bonded layered material (aka basalt flows) near the surface [e.g., Mueller and Golombek, 2004; Golombek and Phillips, 2010].

The thermophysical properties of the landing site indicate that the soil that makes up the surface material is similar to common weakly bonded soils on Earth and conducive to penetration by the heat flow probe. The thermal inertia of the landing ellipse is about  $200 \text{ J m}^{-2} \text{ K}^{-1} \text{ s}^{-1/2}$ , the albedo is 0.25, and dust cover index is 0.94 [see Golombek *et al.*, 2013b, this-issue and references for sources therein]. Comparison with the thermal inertias of existing landing sites and the soils present [Golombek *et al.*, 2008] suggests the InSight surfaces are composed of cohesionless sand or low cohesion soils with bulk densities of  $\sim 1000$ - $1600 \text{ kg m}^{-3}$ , particle sizes of  $\sim 0.15$ - $0.25$  mm (medium to fine sand), cohesions of less than a few kPa, and angle of internal friction of  $30$ - $40^{\circ}$ . Albedo and dust cover index are similar to dusty and low-rock abundance portions of the Gusev cratered plains, which have been dominantly shaped by impact and eolian processes [Golombek *et al.*, 2006]. Mapping of surface terrains in high-resolution images of the landing site and surrounding areas, shows these terrains are also dominantly formed by impact and eolian processes [Wigton *et al.*, 2014; Warner *et al.*, this issue]. At the 100 m scale of the highest resolution thermal inertia, there is no outcrop and no dust cover greater than a couple of mm thick. Seasonal analysis of thermal properties indicate the same materials and physical properties are present down to  $\sim 0.5$ -1 m depth [Piqueux *et al.*, 2014].

The landing ellipse is located on smooth, flat terrain that generally has very low rock abundance [Golombek *et al.*, 2014, this issue]. Most rocks at the landing site are concentrated around rocky ejecta craters larger than 30-200 m diameter, but not around similarly fresh smaller craters [Golombek *et al.*, 2013b; Warner *et al.*, this issue]. Because ejecta is sourced from shallow depths,  $\sim 0.1$  times the diameter of the crater [Melosh, 1989], the onset diameter of rocky ejecta craters can

be used to map the thickness of the broken up regolith. Results indicate a regolith that is 3-17 m thick [Warner *et al.*, 2014, this issue; Pivarunas *et al.*, 2015], that grades into large blocky ejecta over strong intact basalts (Figure 2) [Golombek *et al.*, 2013b]. Because craters larger than 2 km do not have rocky ejecta, material below the basalts at ~200 m depth likely consists of weakly bonded sediments.

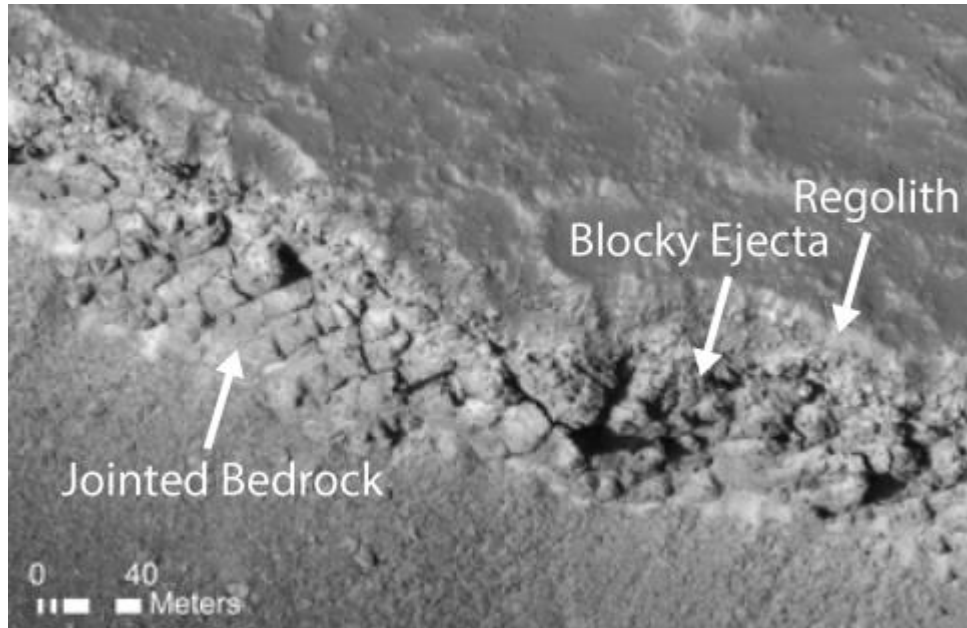


Figure 2. An example of the shallow structure of the InSight landing site. HiRISE image PSP\_002359\_2020 of a portion of the Hephaestus Fossae in southern Utopia Planitia at 21.9°N, 122.0°E showing ~5 m thick, fine grained regolith, that grades into coarse, blocky ejecta that overlies strong, jointed bedrock (arrows show each).

## 2.2 The HP<sup>3</sup> probe hammer mechanism

The HP<sup>3</sup> mole has an internal hammering mechanism that compresses a spring and releases a hammering mass every ~3 s, providing kinetic energy for forward motion. This, with reaction force either provided by the support structure (at the beginning) or by the surrounding soil (after the mole has penetrated about one-half body length), drives the mole forward into the soil at a rate of between 3 and <0.1 mm per strike (slower when deeper [Poganski *et al.*, this issue]).

The principle of operation is described e.g., in Grygorczuk *et al.* [2011] and Seweryn *et al.* [2014] and is illustrated in Figure 3. Working as a mechanical diode, momentum is preferentially directed into the direction of the required motion. It is essential for penetration that the external forces balance the backward (recoil) force transferred to the casing by the compression of the brake-spring. The balance between forward and recoil forces depends on the ratios between the hammer and suppressor-mass, mass of the casing, the properties of the springs, and the hull/soil friction force. For the present mole, a force balancing the recoil of 5-6 N is required. Under certain unfavorable conditions – e.g., the mole hitting a very hard surface and the suppressor mass directly hitting the casing on the upward motion (compare Fig. 3, step 5) – a force of up to 6.7 N may be required. This is the maximum force of the brake-spring. The design of the mole assumes that the balancing force is provided by friction between the soil and the outer hull. Initially, when the mole is only partly inserted and comparatively little friction is available, a mechanical support system is used.

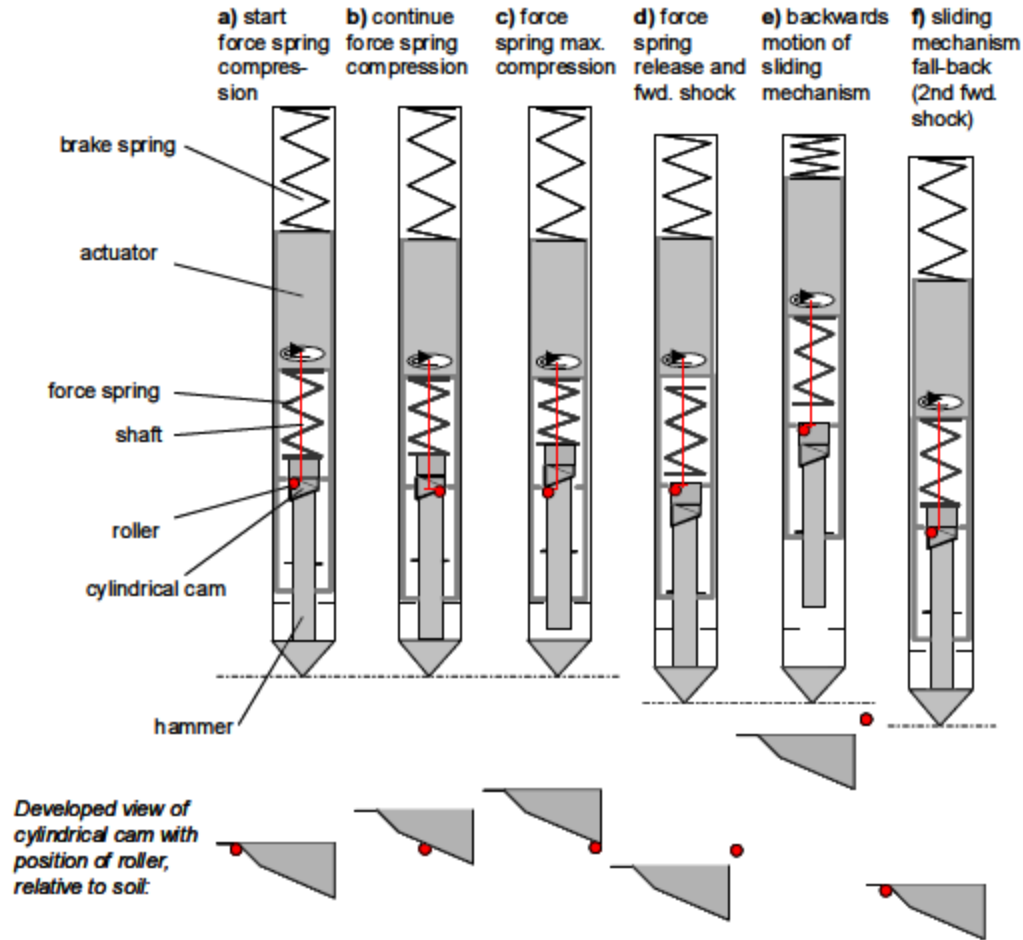


Figure 3: The HP<sup>3</sup> mole mechanism. In the hammering mechanism, a motor provides rotational motion that is converted by a gearbox into translational motion of a piston to compress the drive-spring (Steps a-c in Figure 3). When the drive spring is released (c), its expansion accelerates the hammer that will hit an anvil connected to the casing to transfer the momentum forward (d). At the time of release of the drive-spring a counter-mass (composed of motor, gearbox, piston, and hammer, and termed 'suppressor-mass') is accelerated and moves upward (e) against the resistance of the brake-spring. This motion transfers momentum backward to the casing that must be absorbed by an external force. The suppressor-mass is then accelerated forward (f) to provide a second hit to the casing. [From Spohn et al., 2012]

### 2.3 The seismic signature of the hammer source

Most of the current knowledge of the signal properties of the seismic signals generated by HP<sup>3</sup> are derived from direct measurements of the impulse carried out in an experimental setting in the JPL test area known as the Mars Yard with an early prototype mole. The mole was placed within a sand pit with embedded high frequency accelerometers recording a series of several hundred hammer impulses at 100 kHz. This measurement provided the necessary information of the source time function (Figure 4), as well as statistical information on the consistency of time intervals between hammer pulses. As explained below this information is later used in numerical simulations of the full experiment in Martian soil, and information about the signal repeatability and time interval.

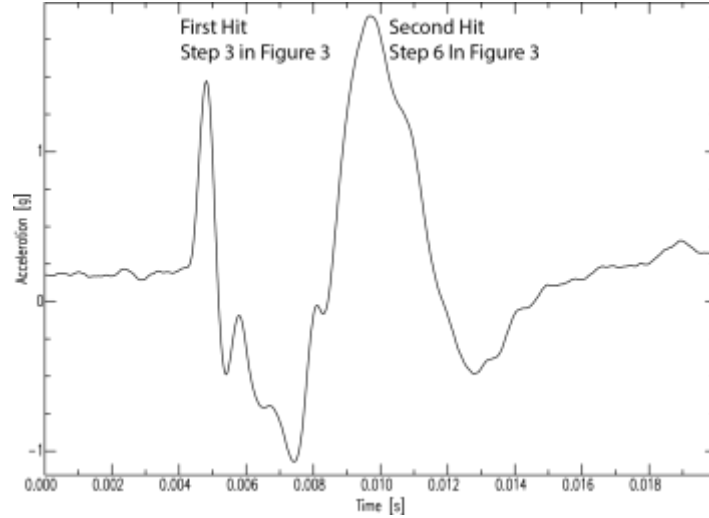


Figure 4: Vertical seismic signature of the HP<sup>3</sup> mole mechanism recorded 0.3 m away. In the Mars Yard experiment the probe tip reached a depth of ~30cm before it was turned off. While the frequency content of the signal did change slightly with depth even over this short distance, but the overall feature of a double pulse is consistent through all the recorded pulses. For the purpose of this study, the above signature is assumed to represent the source time function. A more careful measurement of the source time function with the latest version of the mole in realistic conditions will be carried out in the future and be implemented in the analysis of HP<sup>3</sup> strokes on Mars.

The amplitude of the direct signal was measured in sand to be about 1 m/s<sup>2</sup> at a distance of 1 m away from the source. Even accounting for a more attenuating medium, the direct pulse from the source will undoubtedly be observed by both InSight's Very Broad Band (VBB) and Short Period (SP) seismometers (Figure 5). In fact, a concern might be that the signal might clip the seismometers. To address this concern, a follow-up field experiment with the latest HP<sup>3</sup> mole design and an Earth version SP and a broadband seismometer will be conducted.

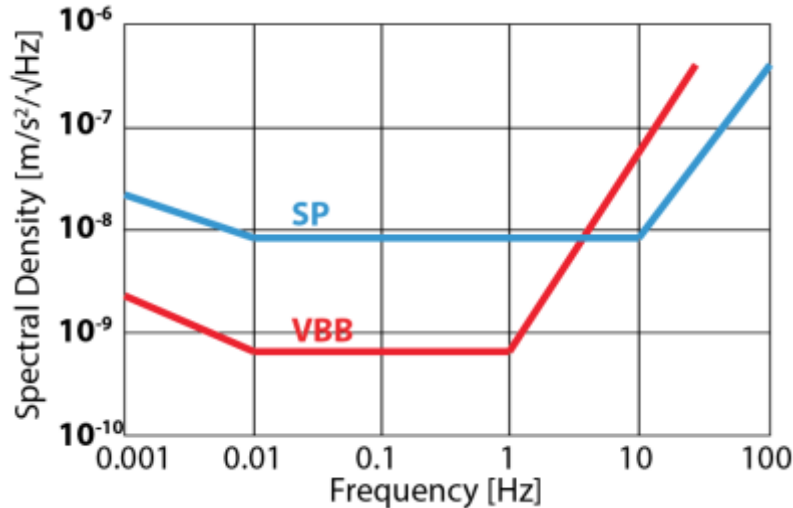


Figure 5: Performance requirements of InSight's vertical VBB and SP sensors

A key observation required to constrain the thickness of the regolith layer is the reflected *P* phase from the presumed regolith-rock interface (See Figure 2). An estimate of the reflected signal amplitude for a ~100 m round-trip off a 50 m deep reflector can be calculated using the measured signal amplitude (Figure 4), and basic assumptions about geometrical spreading and attenuation.



The amplitude  $A$  of a signal reflected from a reflector at depth  $d_R=50$  m, with a calculated near vertical reflection coefficient up to  $C_R \sim 0.8$  from the regolith-rock interface (see Table 1, Section 3.1), and a wavelength  $\lambda \sim 5$  m would be:

$$A(2d_r) = A_0 e^{-2\pi d_R/\lambda Q} \frac{1}{4\pi(2d_R)} C_R$$

The reflected signal strength thus calculated to be  $10^{-8}$ – $10^{-4}$  m/s<sup>2</sup> assuming the frequency content of the signal shown in Figure 4 at the source, and a Quality factor,  $Q$ , of 10-100 respectively. The reflection coefficient is based on the assumption of a sharp boundary. Naturally, it would be smaller if the transition between the regolith and the hard rock below it is diffuse.

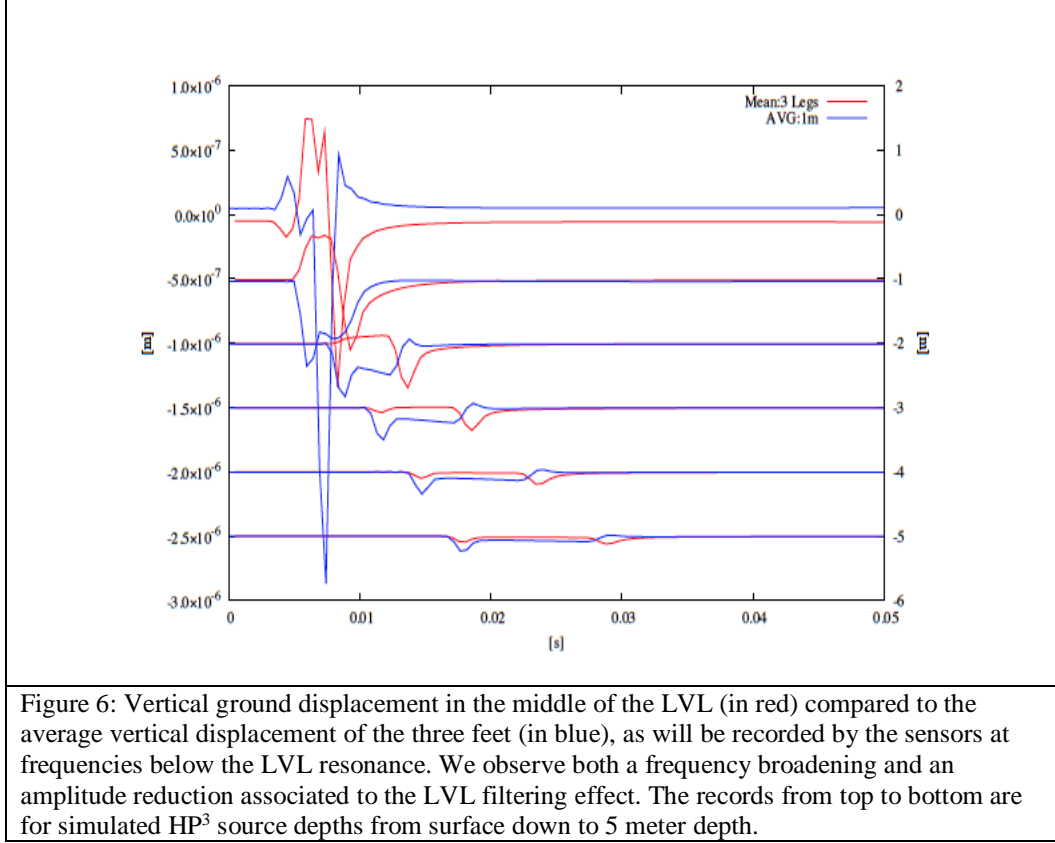
Both the VBB and SP sensors are expected to record high frequency wind generated seismic noise in the planetary boundary layer [Teauby *et al.*, this issue]. The amplitudes are unknown but are expected to generate the high frequency noise floor of the HP<sup>3</sup> seismic records for both the SPs and the VBBs. As will be discussed below, taking advantage of the multitude of hammer strokes and the knowledge of the hammer timing will help enhance the signal-to-noise-ratio (SNR) of the hammer seismic signal.

Having both SP and VBB high frequency record of the HP<sup>3</sup> hammering may introduce some interesting possibilities: (1) Since the three VBB and SP sensors are located at different distances from the SEIS center of mass recording a total of 6 axes of motion, it may enable rotational seismic measurements; (2) By possibly “interleaving” the VBB and SP channels, the HP<sup>3</sup> signals may be recorded effectively at 200 Hz. This can be done by introducing a 5 ms phase delay of all VBBs with respect to all SPs. If implemented, this approach will have to be applied after the first penetration signals when the 6 axis response of the seismometer leveling system (LVL) will have been monitored with enough resolution by all inertial sensors.

## 2.4 Resonance in the SEIS self-Leveling (LVL) System

The connection between the SEIS sensors and the Martian ground is provided by the leveling system (LVL). The purpose of the LVL is two-fold: to ensure leveled placement of the sensors under yet unknown deployment conditions on slopes of up to 15° in arbitrary orientation likely strewn with small surface rocks, and to provide a good coupling between the sensors and the ground. The LVL design consists of three linear-actuator legs on a frame that carries SEIS instruments. The legs can be commanded to move independently to allow level placement on a sloping ground surface. The cone-shaped feet of the LVL sink into the Martian regolith during deployment up to a disk on top of each foot that prevents further sinking, resulting in stable coupling to the ground.

The three leg configuration has, however, some impacts in the high frequency measurements of the HP<sup>3</sup> signals, as they average the ground acceleration sensed across the three feet. The feet are located on the diameter of a 250 mm ring, at distance of about 215 mm. For the very low seismic velocities of the subsurface, this is corresponding to half of the wavelength of an S wave of about 400 Hz (for S waves velocities of 173 m/s). The LVL is therefore acting as a first order high pass filter, with a 400 Hz cutoff frequency. This effects is shown in Figure 6, where the ground displacement at the center of the 3 feet is compared to the average of the 3 feet, for signals recorded from the surface to 5 meter depth. This effect will likely reduce the amplitude of the signal by factor of  $\sim 2.5$  at the beginning of the penetration phase, down to amplitude of about 1 micron of ground displacement. Such amplitudes are not expected to saturate the first stage of the acquisition system (with large margins for both the SP and VBBs low gain mode) and will therefore provide high signal to noise output for both the SPs and VBBs, enabling the search for reflections from subsurface interfaces.



During the performance tests it was found that the elevated-tripod structure of the LVL shows significant resonances in horizontal directions that will affect signals recorded by the SEIS sensors. We measured the resonance frequency in the laboratory using an LVL system and a representative seismometer mass. Resonance frequencies were shown to depend primarily on the extracted lengths of the legs, and range between 35 Hz and 45 Hz in tests conducted at various tilts up to 15°. In a realistic deployment scenario, the resonance frequencies may increase slightly as the LVL feet are embedded in the soil. The most significant effect is an amplification of horizontal motion at resonance frequencies. Recordings of the vertical component show no conclusive evidence of LVL resonances. Vertical amplification, if any, is about two orders of magnitude less than on the horizontals.

Figure 7 illustrates the resonance effects on the horizontal components, for two resonance scenarios at 68 Hz or 38 Hz and Q of either 25 or 100. These resonances will generate ringing, as well as some overshoot of the signal. For resonances above 50 Hz, the overshoot will significantly increase the amplitude of the signal prior to its entering the digital acquisition chain, risking saturation of the Analog-to-Digital (A/D) conversion. This will impact the SPs than the VBBs, as they have a flat output in velocity and displacement, respectively. These ringing effect will furthermore need to be corrected by an LVL transfer function, in order to enable the seismic analysis presented in later sections of this paper. They furthermore will interfere with the identification of reflected arrivals on the horizontal components. A detailed model of the LVL transfer function is developed further by *Fayon et al* in a separate paper.

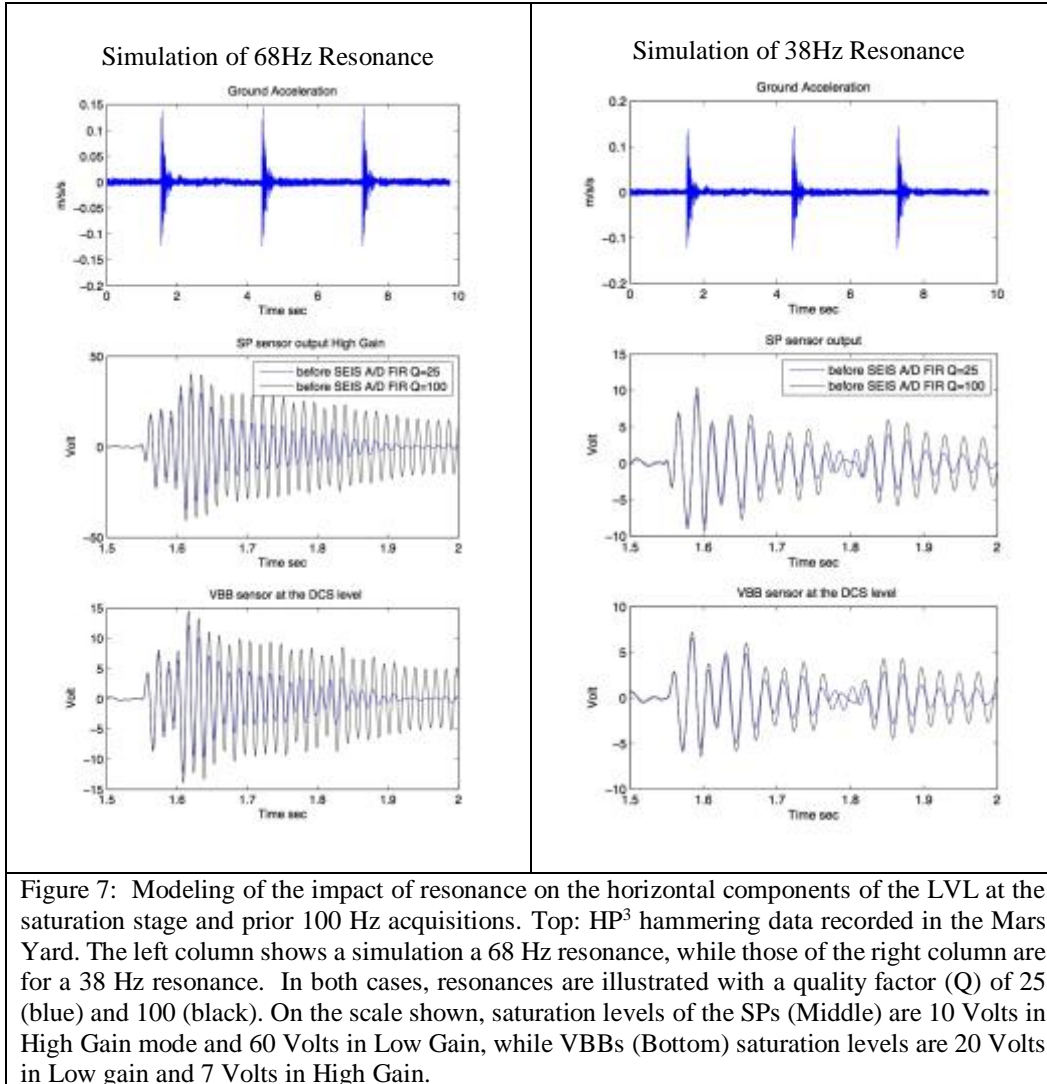


Figure 7: Modeling of the impact of resonance on the horizontal components of the LVL at the saturation stage and prior 100 Hz acquisitions. Top: HP<sup>3</sup> hammering data recorded in the Mars Yard. The left column shows a simulation a 68 Hz resonance, while those of the right column are for a 38 Hz resonance. In both cases, resonances are illustrated with a quality factor (Q) of 25 (blue) and 100 (black). On the scale shown, saturation levels of the SPs (Middle) are 10 Volts in High Gain mode and 60 Volts in Low Gain, while VBBs (Bottom) saturation levels are 20 Volts in Low gain and 7 Volts in High Gain.

## 2.5 HP<sup>3</sup> Signal timing

SEIS and HP<sup>3</sup> are not connected via a direct communication line. A correlation of measurements of the two experiments has to be performed via their respective internal clocks via the spacecraft clock. Each HP<sup>3</sup> hammer stroke is to be detected by an internal measurement suite known as STATIL - a subsystem located inside the mole, dedicated to determining the inclination of the mole vs the gravity vector, and composed of two 2-axis accelerometers (ADXL203 from Analog Devices). These sensors have a dynamic measurement range of  $\pm 1.7$  g. STATIL measures the mole inclination in-between the hammering strokes. The measurement itself is triggered by the detection of the acceleration of mole stroke. The STATIL recording starts exactly 1 s after being triggered event by the sensor. In this way the stroke measurement is recorded indirectly in the timestamps of the STATIL measurement.

The STATIL accelerometer output voltages are recorded by the HP<sup>3</sup> back-end-electronics (BEE) with a frequency of 600 Hz. This 6 times faster than SEIS data logging rate, and therefore results in a high resolution timing of the source. Since the STATIL measurements recording starts 1

second after the trigger level of the stroke edge has been reached, the time of the stroke event can be determined based on this timestamp.

### 3. Data analysis of the HP<sup>3</sup> seismic record

#### 3.1 Simulation of seismic data from HP<sup>3</sup>

In order to develop the analysis tools that will be applied to the HP<sup>3</sup> seismic data we simulated a sample data set of seismograms generated by a hammer stroke. We model the process by assuming a 1 mm penetration of the HP<sup>3</sup> mole per hammer stroke down to 5 m, generating in total 5000 seismograms and using the normal mode summation technique of *Herrmann* [2013]. We assume a 1 m surface separation between HP<sup>3</sup> and SEIS. We further assume a subsurface model of a 50 m soft layer over a harder half-space as described in Table 1. These values are used in all subsequent numerical models.

Thickness (m)	V <sub>p</sub> (m/s)	V <sub>s</sub> (m/s)	ρ (kg/m <sup>3</sup> )	Q <sub>p</sub>
50m	300	173	1500	50
Half-space	2000	1154	2700	100

Table 1: Subsurface seismic properties used to generate synthetic seismograms. The values for the regolith layer are in agreement with laboratory tests of regolith simulant conducted by *Delage et al.* [2016 – this issue].

To simulate more closely the InSight seismograms, we subsample the seismograms down to 100 Hz, mimicking the input data sampling rate (500 Hz). Subsequently we apply the decimation algorithm used by the InSight digitizer, resulting in an InSight-like 100 Hz seismogram (Figure 8).

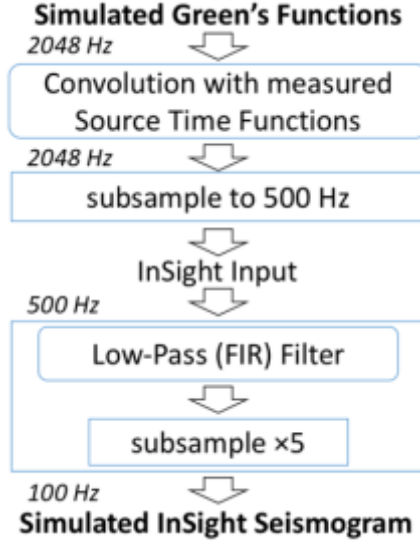


Figure 8: Generation of simulated 100 Hz InSight Seismograms. Green's functions at 2048 Hz, are produced using a normal mode summation program [Herrmann, 2013]. These are convolved with the measured Source Time Function (Figure 4) and are subsampled to generate the 500 Hz simulated raw InSight input data. Subsequently, InSight's anti-aliasing FIR filter is applied and the signal is further subsampled to 100 Hz to create a set of simulated InSight seismograms.

A comparison between the high-frequency seismograms (Green's functions convolved with the measured Source Time Function (Figure 4), and the final decimated data is shown in Figure 9.

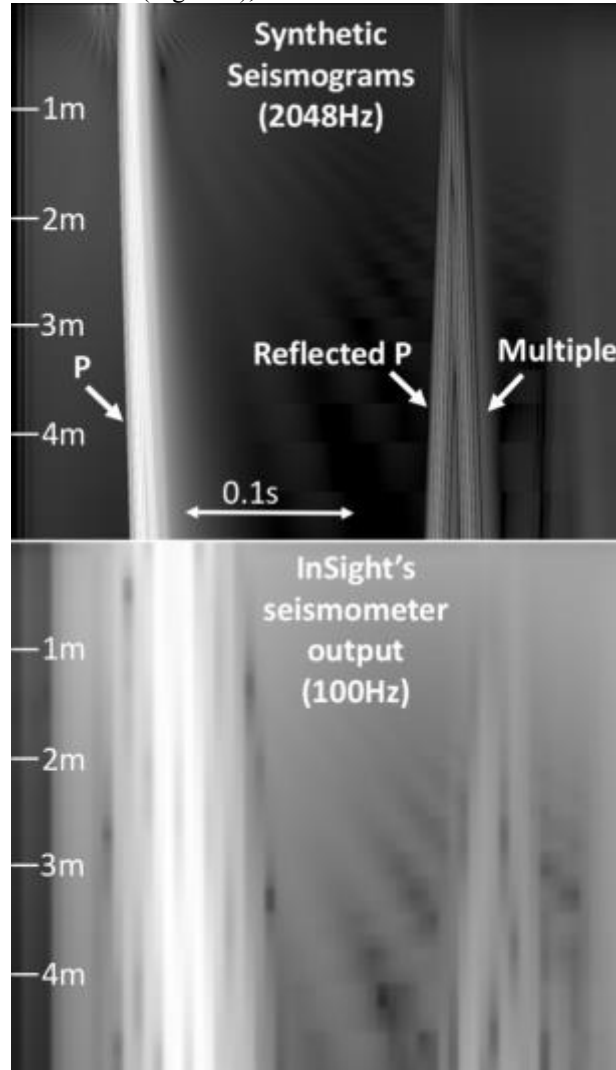


Figure 9: Composite image made of 5000 seismograms at high resolution (Top, 2048 Hz) and as they would be observed by InSight (Bottom, 100 Hz). The seismograms are independently normalized at each depth, with intensity proportional to the logarithm. Note that some numerical noise is enhanced by the logarithmic scaling in the plot, creating the false appearance of a-causal energy arrival. This effect is worsened by the down-sampling to 100Hz.

## 3.2 Information recovery

In this section we describe several potential methodologies for recovering information about Mars's shallow interior from under-sampled data, using the down-sampled data described in Figure 9 to reconstruct the higher frequency signal and ultimately the velocity structure of the regolith layer under SEIS.

### 3.2.1 Signal Recovery

Since SEIS data is sampled at 100 Hz information above 50 Hz is potentially lost. Nevertheless, using the information obtained from empirical measurements of the source time function (Figure 4) it may be possible to recover information above the 50 Hz Nyquist frequency.

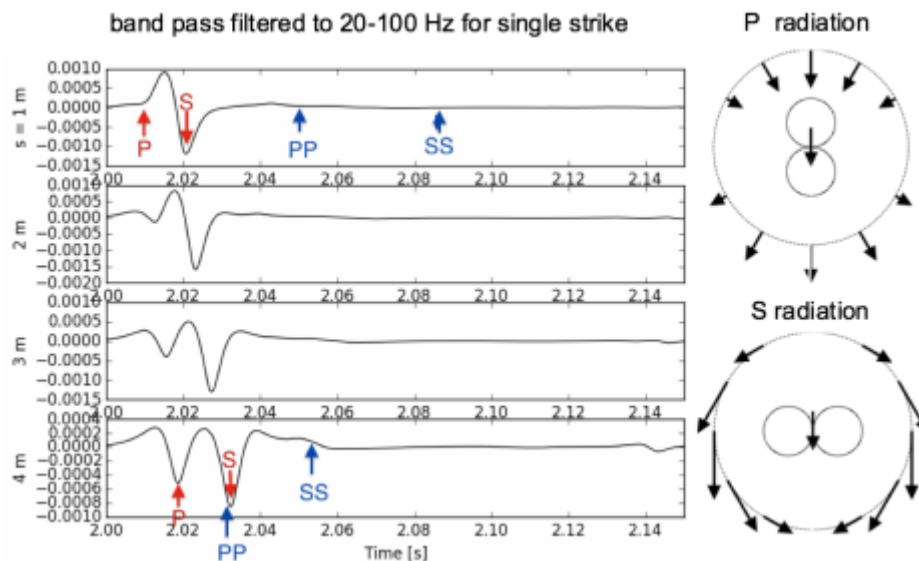


Figure 10: Left: Synthetic signals band pass filtered from 20-100 Hz at a high sampling rate. Four synthetic seismograms are calculated using SPEC3D with force sources located at depths of 1 m, 2 m, 3 m, and 4 m. Visible arrival of seismic phases are labeled. Right: Source radiation pattern of a single downward strike for P and S waves.

Consider the pre-sampled seismograms simulated in Figure 10. Because hammering the HP<sup>3</sup> mole down to 5 m underneath the landing site is a fairly slow process, signals excited within a relative short period of time are highly similar, since the repeat rate of hammering is about 3 seconds, and the speed of the mole is about 0.1 - 1 mm/stroke. Therefore, within a ~30-minute hammering session the hammering process can generate more than a thousand signals while the source migrates approximately 10 cm. Depending on the relative position of the HP<sup>3</sup> mole and SEIS, and the precise timing of a hammer stroke, different hammer strokes may be sub-sampled differently. Even consecutive shots may appear distinctly different from each other (Fig. 11). To pick these distinct under-sampled signals and reconstruct the complete waveforms we first down-sample the source time function (Figure 4) at the same low 100 Hz sampling rate (Fig. 12). For a 0.1-second-long source time function, down-sampling from 800 Hz to 100 Hz is equivalent to selecting 10 data points at 0.01 second time spacing out of 80 data point at 0.00125 second spacing. This approach results in eight different waveforms with a 0.0025 second time shift after down sampling (Fig. 12).

The eight down-sampled signals are then used as reference signals to pick similar signals from raw data via correlation. For each reference signal, we select the signals in the record with cross-correlation coefficient above a certain threshold value (0.6 in this example) and stack them to form a mean signal. Combining the eight mean signals at a 100 Hz sampling rate, we can reconstruct the complete waveform at 800 Hz, as shown in Figure 13. The success of this method depends upon high repeatability of hammer stroke signals. The repeatability of hammering source time function will be investigated in future experiments. Since the change in depth between strokes is minimal (~1mm), the waveform will change very gradually (Figure 9). A good reference signal is also critical for the cross-correlation approach to recover the complete mean signals. In addition to the theoretically calculated reference signal, field data from the Mars Yard and elsewhere will be used as templates to correlate with the Insight data for signal recovery.

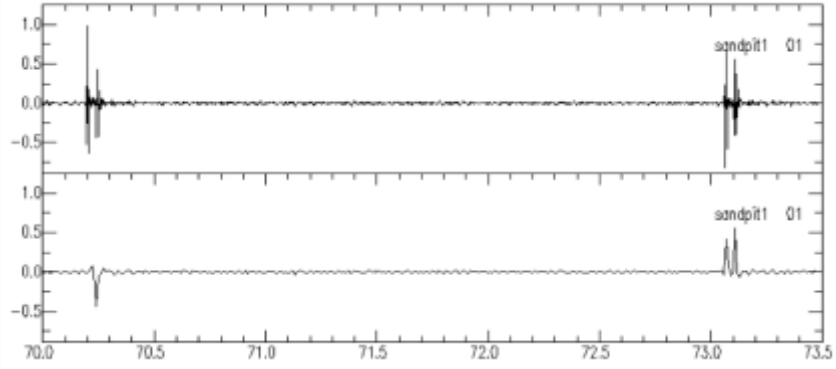


Figure 11: Top: Two consecutive signals at 400 Hz sampling rate recorded in the field; Bottom: signals down-sampled to 100 Hz.

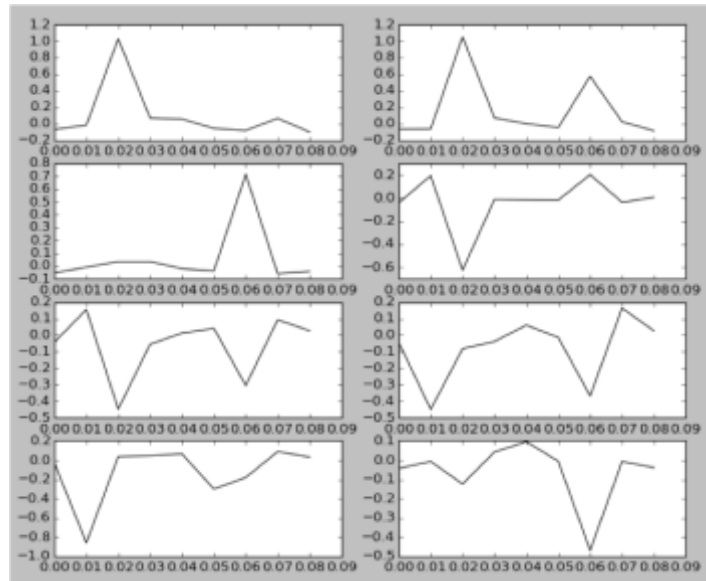
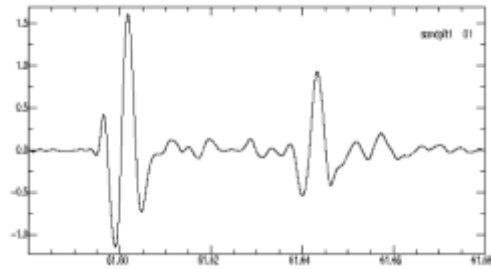


Figure 12. Top: two consecutive signals at 800 Hz sampling rate recorded in the field; Bottom panel: signals down sampled to 100 Hz with an even time shift (0.0125 sec).

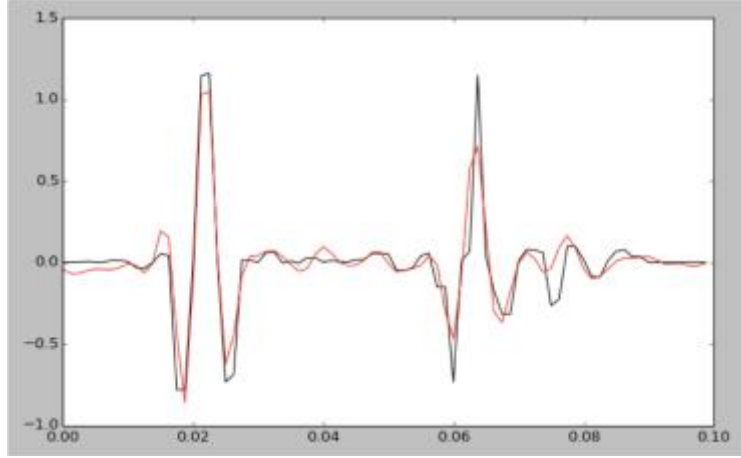


Figure 13. Comparison between original signal (black) and recovered signal (red).

### 3.2.2 Signal Stacking

The HP<sup>3</sup> mole will reach its target depth of 5 m by many small incremental movements of approximately 0.1-1mm per hammer stroke, depending on regolith properties. This will lead to a large number of very similar seismic traces, which will slowly evolve as the mole penetrates the regolith. The resulting dataset will be somewhat analogous to compact array seismology on Earth, where seismograms for a single event recorded on multiple stations are stacked to increase the signal to noise ratio [Schweitzer *et al.* 2012]. For the HP<sup>3</sup> mole, we will instead be stacking multiple similar events recorded on a single station, but the same techniques can be applied. This will enable much fainter arrivals to be detected than would otherwise be possible. For example, weak reflections from the bottom of the regolith layer or bedrock refractions can be detected. The principle of reciprocity states that source and receiver positions are interchangeable (e.g. *Aki and Richards* 2002), thus the mole dataset will be equivalent to a single surface source (at the SEIS location) with a vertical array of receivers along the mole trajectory. This will allow crude vertical seismic profiling, as is commonly employed in borehole seismology, to be applied to the upper regolith layer.

Stacking methods for array seismology are reviewed by *Rost and Thomas* [2002] and *Schweitzer et al* [2012]. To stack a signal effectively the seismic traces from multiple hammer strokes must be sufficiently similar so that a coherent signal is enhanced, while incoherent ambient noise is suppressed. This is the case across small seismic arrays where the epicentral distance is large compared to the array spacing, or in our case for traces where the mole remains in a narrow enough depth range for the signals to be indistinguishable. Assuming this condition is satisfied there are a number of simple stacking methods that could be applied.

**Linear stack:** The linear delayed-sum stack is the simplest stacking method and is widely employed. Consider a set of  $M$  individual traces  $w_j(t)$ , where the index  $j=1 \dots M$  indicates the trace number. The linear stack  $b(t)$  is defined by:

$$(1) \ b(t) = \frac{1}{M} \sum_{j=1}^M w_j(t + \Delta t_j)$$

where  $\Delta t_j$  are the delay times for each trace. Sub-sample level values for  $\Delta t_j$  are possible if the trace is interpolated. In the presence of uncorrelated Gaussian noise, the linear stack gives an improvement in signal to noise ratio by a factor of  $\sqrt{M}$ . The linear stack also preserves the shape of the arrival waveforms, so can be used for amplitude studies.

**$n^{\text{th}}$ -root stack:** The  $n^{\text{th}}$ -root stack involves taking the sign-preserving  $n^{\text{th}}$  root, then performing a delayed-sum stack to give  $b'(t)$ , followed by taking the  $n^{\text{th}}$  power and preserving the sign to give the final stack  $b(t)$  [McFadden *et al.* 1986, *Rost and Thomas*, 2002].



$$(2) \quad b'(t) = \frac{1}{M} \sum_{j=1}^M |w_j(t + \Delta t_j)|^{\frac{1}{n}} w_j(t) / |w_j(t)|$$

and

$$(3) \quad b(t) = |b'(t)|^n b'(t) / |b'(t)|$$

This stacking method is much more sensitive to trace coherence than the linear stack and is better at emphasizing faint arrivals. However, it distorts the waveforms and so cannot be used for waveform shape or amplitude studies. There are also more complex non-waveform conserving methods such as semblance, phase weighted, and f-statistic stacking [Rost and Thomas, 2002; Schweitzer et al., 2012].

For terrestrial array seismology, which typically has good timing and event information,  $\Delta t_j$  can be calculated for each trace using the event back azimuth and the horizontal slowness of the arrival. However, on Mars this may not be possible especially if we did not rely on the STATIL trigger time (See section 1.5). Therefore,  $\Delta t_j$  can be inverted for using a technique similar to that presented in Rawlinson and Kennett [2004]. If the individual seismograms have relatively high signal to noise ratio this could be a simple cross correlation based on a master event as described above (Section 2.2.1). For noisier seismograms where the arrivals have a similar level to the ambient noise, then the relative delays can be inverted for to maximize the energy in the stack.

**Stacking requirements:** During the stacking process care must be taken to ensure the required signals are in phase for all traces. For example, consider the arrival for the direct P-wave and the arrival for the P-wave reflected from the bottom of the regolith layer. The relative timing of these two phases will change as the mole increases in depth (Fig. 9), so a stack aligned on the direct phase will result in the reflected phases being misaligned, becoming incoherent between traces, and resulting in a washed out stack.

In practice the simplest way to ensure that all arrivals are in phase is to perform a series of separate stacks, each with a limited range of mole depths. We can gain an approximate estimate of the depth-slice requirements using simple ray tracing. Consider a mole with depth  $z$  and horizontal distance  $x$  from the SEIS instrument, with a uniform regolith layer of depth  $H$  and P-wave velocity  $v_r$ . The travel times of the direct wave  $t_p$  and the reflected wave  $t_{pp}$  are given by:

$$(4) \quad t_p = (x^2 + z^2)^{1/2} / v_r$$

and

$$(5) \quad t_{pp} = [(2H - z)^2 - x^2]^{1/2} / v_r$$

The travel time difference between the two arrivals is  $\tau = t_{pp} - t_p$ . For the stack to be coherent in both arrivals  $\tau$  must be less than some tolerance  $\delta t$ , which we choose as  $1/16^{\text{th}}$  of the sampling interval to ensure that phase differences are less than  $1/16^{\text{th}}$  of the lower pass filtered waveform. The SP sample rate is 100 Hz, which gives  $\delta t = 0.625$  ms. Figure 14 shows the depth range that can be included in a stack to satisfy this requirement assuming a 1 m horizontal separation between the mole and SEIS.

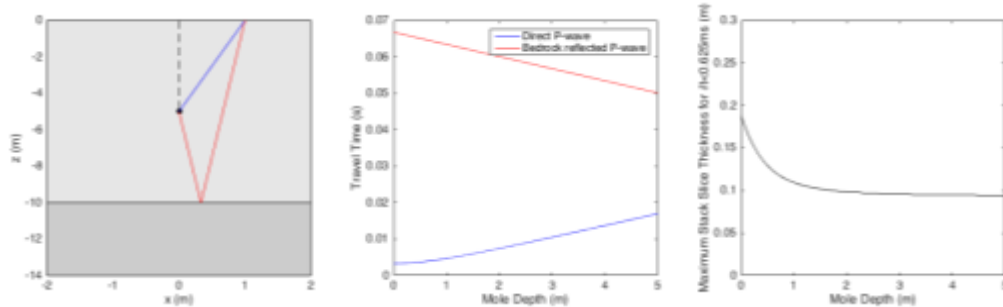


Figure 14: Stack depth slice requirements for a uniform regolith layer with a P-wave velocity of 300 m/s and a depth to bedrock of 10 m. (a) Sketch of ray paths for direct and reflected P-wave. (b) Travel time curves. (c) Maximum depth slice thickness over which traces can be stacked to ensure  $1/16^{\text{th}}$  sample interval coherence of both reflected and direct phases.

Therefore, for a reasonable regolith velocity of 300 m/s a slice  $\sim 0.1$  m thick can be stacked. In laboratory tests using a 5 m high sand tank, an average hammer strike moves the mole  $\sim 1$  mm, so

on average  $\sim 100$  strikes can be stacked without introducing significant phase differences between different arrivals. This will result in an increase in signal to noise of  $\sim 10$ .

### 3.2.3 Determining seismic velocities

As seen in figure 9 (Bottom) Once the signal is sub-sampled the  $S$  and  $P$  arrivals are blurred into a single arrival, with an apparent average velocity. The reflection from the regolith base is still observable. The challenge for the recovery algorithm is to determine the timing and slopes of both arrivals. This is done using a two-step algorithm: The first step recovery is an approximation to the 500 Hz input signal (Figure 8) via the methods described above or using a *sinc*-function interpolation (Figure 15). Subsequently, provided that the 500 Hz input signal can be recovered with high fidelity, we proceed to estimate the movement of the combined  $S+P$  waves and the reflected P-wave ( $R_p$ ) as follows.

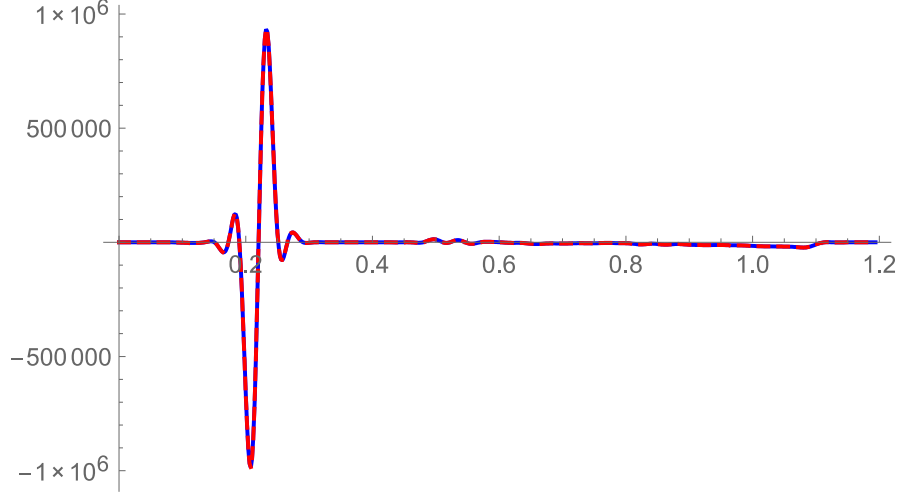


Figure 15: an Example of a Sinc function interpolation of the simulated InSight 100 Hz output signal (Blue dotted line) demonstrates the input 500 Hz signal (Red solid line) can be reliably recreated.

Let  $z(d,t)$  denote the reconstructed sample at depth  $d$  and time index  $t$ ,  $Z(d)$  denote the vector of all such samples at depth  $d$ , and  $\|Z(d)\|$  denote the L2 norm of this vector. For a fixed time index  $t$ , we find the depth value  $d$  that maximizes a smoothed version of  $z(d,t)/\|Z(d)\|$  (Figure 16).

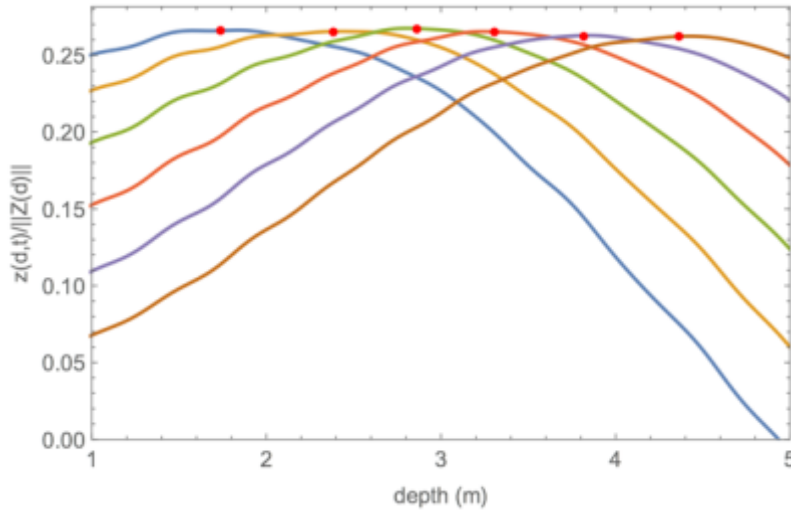


Figure 16: Tracking S+P. Example of six consecutive time indices 0.222s – 0.232s, 0.002s apart are plotted and their maxima is calculated. These maximum (red) points correspond to the approximate depths where  $z(d,t)/\|Z(d)\|$  is maximized for different time indices.

To determine the reflected  $P$ , at a given depth  $d$ , we locate a time value  $t$  corresponding to a local maximum of  $|z(d,t)|$ . This procedure is repeated at the next depth value, finding the local maximum closest to the one found at the previous depth value. This gives us a sequence of (time, depth) values which (if our initial peak was well-chosen) approximately correspond to direct  $P$ , and Reflected  $p$  (Figure 17).

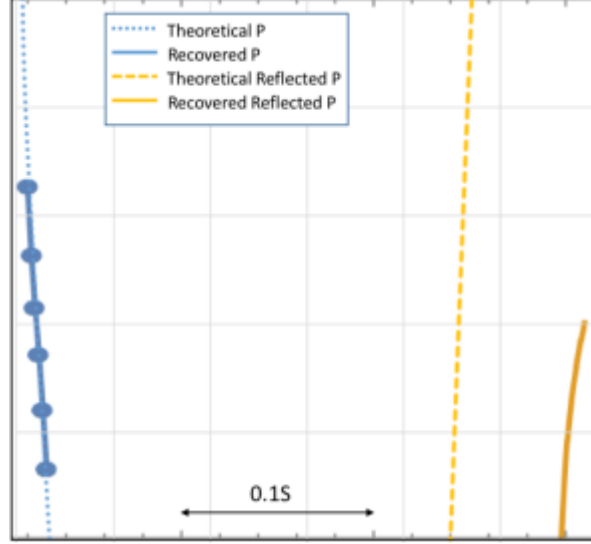


Figure 17: The recovered direct  $P$  and reflected  $P$  using the algorithm described above. The relative delay of the reflected  $P$  phase is attributed to the blurring of the synthetic seismogram with the convolution with the Source Time Function and sub-sampling. The delayed reflected  $P$  results in a  $\sim 20\%$  error in the reflected depth, but can be corrected using pre-launch knowledge of the Source Time Function.

### 3.2.4 Attenuation Profiling

Seismic attenuation is the dissipation of energy through friction or non-elastic deformation and affects the amplitude of seismic signals propagating through natural materials. Attenuation is quantified using the seismic quality factor  $Q$ , where the amplitude attenuation factor for propagation distance  $r$  at frequency  $f$  through a medium with seismic velocity  $v$  is  $\exp(-\pi f r / v Q)$  [Shearer, 2009].

The impulsive hammer strikes of the HP<sup>3</sup> mole result in a very high frequency source waveform. Analogue experiments using a flight spare in the JPL Mars Yard allowed determination of the source waveform (Figure 4), which has a dominant frequency of  $\sim 50$ -200 Hz. Therefore, given the high seismic frequencies and likely low  $Q$  value of unconsolidated regolith, the mole seismic signal will be highly affected by attenuation.

This sensitivity may allow  $Q$  profiling of the upper regolith. However, the viability of this will depend on having a sufficiently low  $Q$  to give a measurable effect in the seismic amplitudes, which will also depend on other factors that control the amplitude. In Fourier space the direct wave amplitude measured by SEIS from the mole at depth  $z$  can be expressed as:

$$(6) \quad A(z,f) = A_0(z=z_{ref},f) S(z,f) D(\theta) K(r,f) G(r)$$

where  $A_0$  is a reference amplitude,  $S(z,f)$  is the source function relative to a reference event source function,  $D(\theta)$  is the source directionality,  $\theta$  is the direction of SEIS measured from the mole forward direction,  $K(r,f)$  is the attenuation at source-receiver distance  $r$ , and  $G(r)$  is the

geometrical spreading. The sample rates of both SEIS-SP and SEIS-VBB will be insufficient to resolve the waveform, but the low pass filtered signal amplitude will be proportional to  $A(z, f)$ . Many of the terms in equation 6 may have a depth dependence. For example,  $S$  will depend on the density of the regolith and the mole confining pressure. Attenuation properties may also vary significantly throughout the regolith layer due to increasing compaction with depth. However, as a first approximation we can model the depth dependence of amplitude by assuming that the source is invariant ( $S=1$ ) and isotropic ( $D=1$ ). An isotropic source radiation pattern may in fact not be too unreasonable as the impact of the mole tip into loose regolith will tend to give an isotropic P-wave radiation pattern akin to an explosive or impact source. Invariance of the source function may also be reasonable once the mole has penetrated the very loose upper layer. For simplicity we also assume a uniform one-layer regolith model with a uniform  $Q$  and seismic velocity  $v_p$ . The geometric spreading can then be approximated by  $G(r) = r_0/r$  and the attenuation is given by  $K(r, f) = \exp(-\pi f(r-r_0)/vQ)$ . Figure 18 shows the variation of amplitude for different values of  $Q$ . If the regolith  $Q$  is less than  $\sim 10$ , attenuation will be the dominant effect on measured amplitude and the amplitude profile could be used to derive attenuation properties as a function of depth. However, for  $Q$  much greater than 10 the attenuation is likely to be too subtle to distinguish from other uncertainties at such small distances.

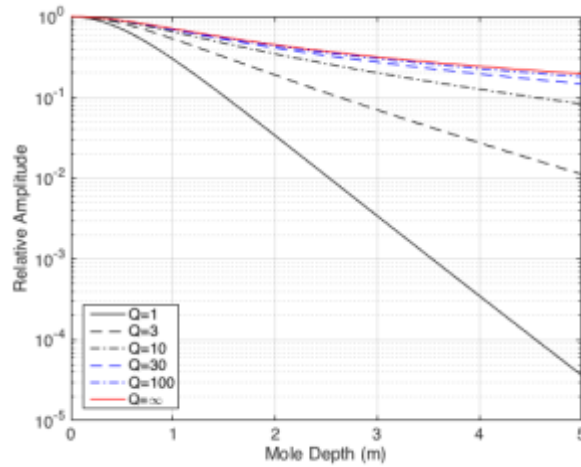


Figure 18: Relative amplitude dependence of the direct P-wave as a function of mole depth for a range of regolith  $Q$  values. Attenuation will be the dominant effect for  $Q < 10$ , whereas for larger  $Q$ s attenuation may be indistinguishable from other effects and it may only be possible to put lower bound on  $Q$ .

A possible complication of the attenuation analysis is the frequency dependence of  $Q$ . At low  $Q$ 's and high frequencies this becomes a significant factor. One possible approach to address this issue would be the analysis of the signal's frequency content as a function of distance from the seismometer after accounting for geometrical spreading.

### 3.2.5 Polarization and H/V analysis

Analysis of regolith depth properties may be enhanced by extracting information from the ambient noise field, specifically from wind generated surface waves. To understand what additional constraint on the shallow subsurface could be provided by the Rayleigh wave ellipticity of ambient vibrations, we calculate synthetic seismograms simulating a random wavefield. We use the parameter values given in Table 1 for the velocity model, and a regolith thickness of 10 m as in the above demonstrations of signal stacking. The wavefield is constructed using a modal summation technique [Herrmann, 2013] for a multitude of randomly distributed and randomly activated impulsive surface sources with random orientations at distances up to 5 km from the seismometer. The sources generate both fundamental and higher mode Love and Rayleigh waves. From the resulting 30-minute long seismograms we estimate Rayleigh wave ellipticity with the

HVTFA method (H/V using time frequency analysis, *Kristekova, 2006; Fäh et al., 2009; Hobiger et al., 2012*). For details, see also *Knapmeyer-Endrun et al. [2016]*.

The above model generates substantial interference with a prominent higher mode, which prevents the extraction of the right flank of the fundamental mode ellipticity peak. Accordingly, we can only derive the left flank of the fundamental mode, the constant level of the fundamental mode at high frequencies, and parts of the higher mode curve (Fig. 19 a)). We use these data as input to an inversion with the Conditional Neighbourhood Algorithm [*Sambridge, 1999, Wathelet et al., 2004*], a direct search algorithm based on Voronoi cells that preferentially samples low-misfit regions of the parameter space. The inversion result is an ensemble of models that can explain the data, thus allowing to estimate uncertainty. The parameter space for the inversion is constrained by a-priori information from the analysis of the HP<sup>3</sup> seismic signals. Based on the estimates provided above, we assume that the true regolith thickness is constrained to  $\pm 20\%$  (Fig. 17), and the average P-wave velocity is known with the same range of uncertainty. Poisson's ratio within the regolith layer as well as within the layer below is assumed to lie between 0.2 and 0.35. A large range is allowed for the sub-regolith velocities, from 800 to 5000 m/s for  $v_P$  and from 500 to 3000 m/s for  $v_S$ . While the actual H/V curve, especially the peak amplitude, is quite sensitive to  $Q$  [*Lunedei and Albarello, 2009; dal Moro, 2015*], the fundamental mode Rayleigh wave ellipticity itself is not.  $Q$  is accordingly no free parameter of the inversion. To derive some information on  $Q$  from the ambient vibration spectra, a complimentary strategy is necessary, e.g. modeling of the H/V curve [*Lunedei and Albarello, 2009*], which requires assumptions on the source distribution and the relative contribution of Love and Rayleigh waves to the wavefield that might be difficult to verify. In addition, density is fixed to sensible estimates (1600 kg/m<sup>3</sup> for the regolith and 2500 kg/m<sup>3</sup> below) in the inversion, as ellipticity is not very sensitive to this parameter.

We run the inversion for 1000 iterations, starting with 250 randomly selected initial models and adding 100 new models in the 100 cells with the lowest misfit in every iteration. We combine results from 5 iterations that use different random seeds to verify the stability of the results. The resulting models that fit the data span the whole range of allowed velocities in the regolith and also the whole range of possible regolith thicknesses (Fig. 19b)). The ellipticity data provide no further constraints on these parameters. However, they do provide some information on the properties of the sub-regolith layer. Velocities in this layer are constrained to 800 m/s to 1400 m/s for  $v_S$ , giving a mean value close to the true value of the model, and 1300 m/s to 2400 m/s for  $v_P$ . This narrows the possible range of velocities in the sub-regolith layer significantly even though the right flank of the fundamental mode could not be used in this inversion. Further examples of how estimates of regolith thickness and average P-wave velocity and ellipticity information can jointly constrain velocities of the sub-regolith layer in more complex models can be found in *Knapmeyer-Endrun et al. [2016]*.

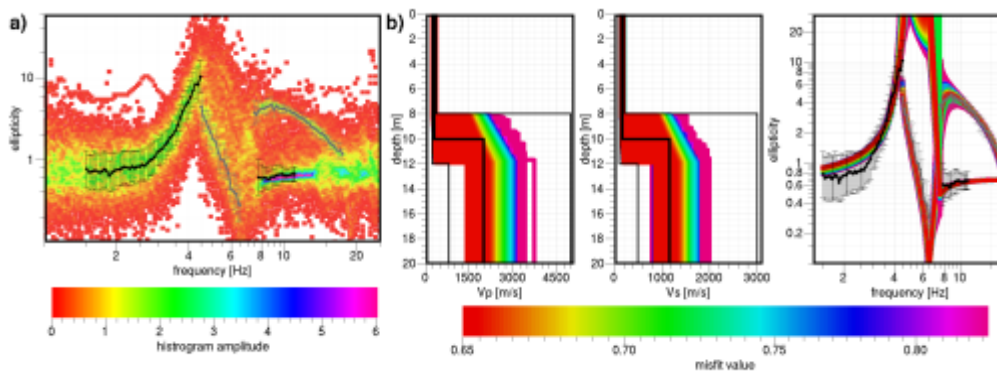


Figure 19: a) HVTFA results showing histogram of ellipticity values found at each frequency. Lines with standard deviations indicate derived ellipticity curves for the fundamental mode (black) and the first higher mode (gray). Note that the right flank of the fundamental mode peak cannot be distinguished in this case; b) Velocity profiles resulting from the inversion of the ellipticity data and fit to the data (right). Thin black lines in the velocity sections outline the parameter space of the inversions and thick black line shows the true model.

## 4. Physical properties and interpretation

### 4.1 Linking seismic measurements to mechanical properties: Density, Strength, Water content, and thermal conductivity

Using measurements of shear and compressional wave velocities, it is possible to infer two independent elastic constants for the regolith, as well as the density of the regolith [Santamarina *et al.*, 2001]. The density of the regolith is a function of porosity and the density of the minerals. On Earth the range for mineral density is quite narrow, where  $2.7 \times 10^3 \text{ kg/m}^3$  is a typical number [Holtz *et al.* 1981]. Mars regolith simulants clearly fall within this range [Delage *et al.*, 1016 – this issue]. SEIS can also be utilized to perform a loading test by a rigid circular plate placed on top of an elastic soil, furnishing in this way a relationship between the pressure on the plate (weight of the instrument by its area), the radius of the instrument, and the elastic constants of the soil and its density [Wood, 2003]. Hence, from two equations of shear and pressure wave velocities, plus one equation relating the SEIS applied as a rigid plate on top of an elastic soil, one can obtain three unknowns: two elastic stiffness constants and the estimated density of the soil. Water content affects the stiffness of the regolith, as well as its mass density. Therefore, potential presence of fluids (though unlikely in the InSight landing site) could be detected by measurements of shear and pressure wave velocity, provided that the water content levels are high enough to be detectable.

The strength of the soil can be characterized by the apparent friction angle and the apparent cohesion. There are empirical relations that can be used, but the preferred approach is to assess the friction and cohesion by using the rate of penetration of the HP<sup>3</sup> instrument in tandem with the impulse generated by the mechanical system of masses inside the mole [Poganski *et al.*, this issue]. The regolith's thermal conductivity can be related to the estimated density [Presley *et al.*, 1997] under Mars conditions. Therefore, there is a tight coupling between the shear and pressure wave velocities, the elastic constants of the soil, the mass density of the soil, the strength parameters of the soil, and the thermal conductivity. Also, the potential presence of fluids would strongly affect all of these properties.

### 4.2 Linking mechanical properties to geological processes and history of Elysium Planitia

The scientific results that can be derived from the seismic analyses described in this paper can also be used to test the geological processes and history that have acted on the landing site in western Elysium Planitia. Our model of the shallow subsurface of the landing site derived from analysis of rocky ejecta craters and images of exposed scarps indicate a regolith that is 3-17 m thick, that grades into large, blocky ejecta over strong intact basalts [Golombek *et al.*, 2016]. The seismic analysis should be able to distinguish if this shallow subsurface model is correct by determining if there is a fine-grained regolith overlying strong, coherent rock. If the analysis does not reveal this structure, then the geologic interpretation of Hesperian basalt flows with an impact generated regolith would need to be revised. However, if the model is correct, the thickness of the regolith can be used to constrain the cratering history, the age of the basalt, the regolith production rate and the effect of other processes that have affected the area. First, the location of the InSight lander in the ellipse can be compared to the pre-landing isopach map of the regolith thickness derived from the onset diameter of rocky ejecta craters [Warner *et al.*, 2016]. As a result, the pre-landing prediction of regolith thickness can be compared directly to the seismic analysis result. Furthermore, because the regolith thickness is a function of the cratering history, the age of the basalt and the effect of other geologic (primarily eolian) processes, which have been estimated by Warner *et al.* [2016]; we can use this comparison to evaluate the relative efficiencies of those processes at this location. In addition, the existence of blocky ejecta between the upper regolith and underlying strong basalt and its thickness are an indication of the relative frequency of craters that just barely excavate down to the intact basalt, compared to the more numerous smaller craters that simply churn the regolith. The expected thickness can be compared to that predicted from the measured size-

frequency distribution of craters in the region. The relative proportion of these different crater diameters can be also used to test the slope of the cratering production function. Finally, the predictions of particle size and maturity index for the fragmentation theory described by the negative binomial function [Charalambous, 2015] applied to the landing site [Golombek *et al.*, 2016] can be tested against the observations of the regolith thickness derived from the seismic analyses.

## 5. Conclusions

InSight's Seismic Experiment for Interior Structure (SEIS) provides a unique and unprecedented opportunity to conduct the first geotechnical survey of Martian soil by taking advantage of the repeated seismic signals that will be generated by the mole of the Heat Flow and Physical Properties Package (HP<sup>3</sup>). Although not part of the stated mission objectives, the HP<sup>3</sup> mole will begin its downward journey into the Martian soil shortly after the commissioning of SEIS, and will therefore generate the first artificial seismic signals ever recorded on Mars. Knowledge of the elastic properties of the Martian regolith have implications to material strength and can constrain models of water content, and provide context to geological processes and history that have acted on the landing site in western Elysium Planitia.

The challenge faced by the InSight team is to overcome the limited temporal resolution of the sharp hammer signals, which have significantly higher frequency content than SEIS 100 Hz sampling rate. Fortunately, since the mole propagates at a rate of ~1 mm per stroke down to 5 m depth, we anticipate thousands of seismic signals, which will vary very gradually as the mole travels. We have also demonstrated that the direct signal, and more importantly an anticipated reflected signal from interface between the bottom of the regolith layer and an underlying lava flow, are likely to be observed by both InSight's Very Broad Band (VBB) and Short Period (SP) seismometers. We have outlined several strategies to increase the signal temporal resolution using the multitude of hammer stroke and internal timing information to stack and interpolate multiple signals, and demonstrated that in spite of the low resolution, the key parameters – seismic velocities and regolith depth – can be retrieved with a high degree of confidence.

The models used in this study to simulate the HP<sup>3</sup>-SEIS geotechnical experiment are encouraging but are limited in their scope. We neglected effects such as a velocity gradient in the regolith layer and a diffuse regolith-rock boundary. Moreover, some concerns regarding clipping of the seismometers and unwanted resonance in its leveling system remain at this time. Therefore, while we continue to tune our models and algorithms, we intend to carry out a full scale field study of the experiment including broad-band seismometers, a terrestrial version of InSight's SP seismometer mounted on the SEIS Leveling system (LVL), and a flight-like mole engineering model. A follow-up report on the field simulation of Mars' first geotechnical study will be published in the future.

## 6. References

- Aki, K. & Richards, P. G. (2002), *Quantitative Seismology, 2nd Ed.*, University Science Books.
- Ansan, V., T. Dezert and the DLT group, 2015, Western Elysium Planitia, What is regional geology telling us about sub-surface? InSight Science Team Presentation, Zurich, Switzerland, September 5-9, 2015.
- Claudio Bagaini and Cesar Barajas-Olalde, Assessment and compensation of inconsistent coupling conditions in point-receiver land seismic data, *Geophysical Prospecting*, 2007, 55, 39–48
- Bonnefoy-Claudet S, Cornou C, Bard PY, Cotton F, Moczo P, Kristek J, Fäh D (2006a) H/V ratio: a tool for site effects evaluation. Results from 1-D noise simulations. *Geophys J Int* 167:827–837. doi:10.1111/j.1365-246X.2006.03154.x

- Catling, D. C., et al., 2011, A lava sea in the northern plains of Mars: Circumpolar Hesperian oceans reconsidered, 42nd Lunar and Planetary Science Conference, abs.# 2529, Lunar and Planetary Institute, Houston.
- Catling D. C., et al., 2012, Does the Vastitas Borealis formation contain oceanic or volcanic deposits? Third Conference on Early Mars, Lake Tahoe, NV, May 21-25, 2012, abs.# 7031, Lunar and Planetary Institute, Houston.
- Dal Moro, G. (2015) Joint analysis of Rayleigh-wave dispersion and HVSR of lunar seismic data from the Apollo 14 and 16 sites, *Icarus* **254**, 338—349, doi:10.1016/j.icarus.2015.03.017.
- Fäh, D., Wathelet, M., Kristekova, M., Havenith, H., Endrun, B., Stamm, G., Poggi, V., Burjanek, J. and Cornou, C. (2009) Using ellipticity information for site characterization, NERIES JRA4 “Geotechnical Site Characterisation”, task B2, D4 - final report ([http://www.neries-eu.org/main.php/JRA4\\_TaskB2\\_D4\\_Final\\_Report.pdf?fileitem=10272807](http://www.neries-eu.org/main.php/JRA4_TaskB2_D4_Final_Report.pdf?fileitem=10272807)).
- Golombek, M. P., et al., 2006, Geology of the Gusev cratered plains from the Spirit rover traverse: *Journal of Geophysical Research, Planets*, 110, E02S07, doi:10.1029/2005JE002503.
- Golombek, M. P., Haldemann, A. F. C., Simpson, R. A., Fergason, R. L., Putzig, N. E., Arvidson, R. E., Bell III, J. F., and Mellon, M. T., 2008, Martian surface properties from joint analysis of orbital, Earth-based, and surface observations: Chapter 21 in, The Martian Surface: Composition, Mineralogy and Physical Properties, J. F. Bell III editor, Cambridge University Press, p. 468-497.
- Golombek, M. P., and Phillips, R. J., 2010, *Mars Tectonics*: Chapter 5 in Planetary Tectonics, T. R. Watters and R. A. Schultz, eds., Cambridge University Press, pp. 183-232.
- Golombek, M., Redmond, L., Gengl, H., Schwartz, C., Warner, N., Banerdt, B., and Smrekar, S., 2013a, Selection of the InSight landing site: Constraints, plans, and progress (expanded abstract) : 44<sup>th</sup> Lunar and Planetary Science, Abstract #1691, Lunar and Planetary Institute, Houston.
- Golombek, M., Warner, N., Schwartz, C., and Green, J., 2013b, Surface characteristics of prospective InSight landing sites in Elysium Planitia (expanded abstract) : 44<sup>th</sup> Lunar and Planetary Science, Abstract #1696, Lunar and Planetary Institute, Houston.
- Golombek, M., Warner, N., Wigton, N., Bloom, C., Schwartz, C., Kannan, S., Kipp, D., Huertas, A., and Banerdt, B., 2014b, Final four landing sites for the InSight geophysical lander (expanded abstract) : 45<sup>th</sup> Lunar and Planetary Science, Abstract #1499, Lunar and Planetary Institute, Houston.
- Golombek, M. et al., this issue, Selection of the InSight landing site, *Space Science Reviews*, in review.
- Grygorczuk, J., M. Banaszekiewicz, A. Cichocki, M. Ciesielska, M. Dobrowolski, B. Kędziora, J. Krasowski, T. Kuciński, M. Marczewski, M. Morawski, H. Rickman, T. Rybus, K. Seweryn, K. Skocki, T. Spohn, T. Szewczyk, R. Wawrzaszek, Ł. Wiśniewski, (2011) Advanced penetrators and hammering sampling devices for planetary body exploration, in: *Proceedings of the ASTRA Conference ESA/ESTEC*, Noordwijk, The Netherlands, 2011
- Herrmann, R. B. (2013) Computer programs in seismology: An evolving tool for instruction and research, *Seism. Res. Lett.* **84**, 108—1088, doi:10.1785/0220110096.
- Hobiger, M., Le Bihan, N., Cornou, C., Bard, P.-Y. (2012) Multicomponent signal processing for Rayleigh wave ellipticity estimation, *IEEE Signal Proc. Mag.* **29**, 29—39, doi:10.1109/MSP.2012.2184969.
- Holtz, R. D., & Kovacs, W. D. (1981). *An introduction to geotechnical engineering* (No. Monograph).
- Knapmeyer-Endrun, B. et al. (2016), Rayleigh wave ellipticity modeling and inversion for shallow structure at the proposed InSight landing site in Elysium Planitia, Mars, *Space Sci. Rev.*, this issue.



- Kristekova, M. (2006), Time-frequency analysis of seismic signals, PhD thesis, Slovak Academy of Sciences, Bratislava, Slovakia.
- Lunedei, E., Albarello, D. (2009) On the seismic noise wavefield in a weakly dissipative layered Earth, *Geophys. J. Int.* **177**, 1001—1014, doi:10.1111/j.1365-246X.2008.04062.x.
- McFadden, P. L.; Drummond, B. J. & Kravis, S. (1986), 'The Nth-root stack: Theory, applications, and examples', *Geophysics* **51**(10), 1879--1892.
- Mueller, K. and Golombek, M. P. (2004). Compressional structures on Mars, *Annual Rev. Earth Planet. Sci.*, **32**, 435–464.
- Piqueux, S., Kleinboehl, A., and Golombek, M. P., 2014, Thermal inertia mapping using climate sounder measurements: Fall Meeting, American Geophys. Un., San Francisco, CA, Dec. 15-19, 2014, Abstract P32A-4021.
- Pivarunas, A., Warner, N. H., and Golombek, M.P., 2015, Onset diameter of rocky ejecta craters in western Elysium Planitia, Mars: Constraints for regolith thickness at the InSight landing site (expanded abstract) : 46<sup>th</sup> Lunar and Planetary Science, Abstract #1129, Lunar and Planetary Institute, Houston.
- Poganski J., · Kömle N.I., ·Kargl G., Schweiger H.F., Grott M., · Spohn T., · Krömer O. · Krause C., Wippermann T. · Tsakyridis G., · Fittock M., ·Lichtenheldt R., ·Vrettos C., · Anrade J.E. (2017, this issue). Extended Pile Driving Model to Predict the Penetration of the Insight/HP3 Mole into the Martian Soil. *Space Sci. Rev.* DOI 10.1007/s11214-016-0302-z
- Presley, M. A., & Christensen, P. R. (1997). The effect of bulk density and particle size sorting on the thermal conductivity of particulate materials under Martian atmospheric pressures. *Journal of Geophysical Research: Planets*, **102**(E4), 9221-9229.
- Rawlinson, N. & Kennett, B. L. N. (2004), 'Rapid estimation of relative and absolute delay times across a network by adaptive stacking', *Geophysical Journal International* **157**, 332-340.
- Rost, S. & Thomas, C. (2002), 'Array Seismology: Methods and Applications', *Reviews of Geophysics* **40**, 1008.
- Sambridge, M. (1999) Geophysical inversion with a neighbourhood algorithm I. Searching a parameter space, *Geophys. J. Int.* **138**, 479—494, doi:10.1046/j.1365-246X.1999.00876.x.
- Santamarina, J. Carlos, A. Klein, and Moheb A. Fam. (2001). Soils and waves: Particulate materials behavior, characterization and process monitoring, *Journal of Soils and Sediments* **1**(2) 130-130.
- Schweitzer, J.; Fyen, J.; Mykkeltveit, S.; Gibbons, S. J.; Pirli, M.; Kühn, D. & Kværna, T. (2012), Seismic Arrays, in Peter Bormann, ed., 'New Manual of Seismological Observatory Practice 2 (NMSOP-2)', Deutsches GeoForschungsZentrum GFZ, Potsdam, pp. 1 - 80.
- Spohn T., M. Grott, J. Knollenberg, T. van Zoest, G. Kargl, S. Smrekar, W. Banerdt, T. Hudson (2012) Insight: Measuring the martian heat flow using the heat flow and physical properties package (HP3). *LPI Contributions* 1683, 1124
- Shearer, P. M. (2009), *Introduction to Seismology*, Cambridge Univ. Press, Cambridge.
- Tanaka, K., et al., 2014, Geologic map of Mars, U. S. Geol. Surv. Sci. Invest. Map 3292.
- Teanby N. A., Stevanovic J., Wookey J., Murdoch N., J. Hurley, Myhill R., Bowles N. E., Calcutt S. B., Pike W. T., Anelastic seismic coupling of wind noise through Mars' regolith for NASA's InSight Lander at short Periods, *Space Science Reviews*, in review.
- Warner, N. H., Golombek, M. P., Bloom, C., Wigton, N., and Schwartz, C., 2014, Regolith thickness in western Elysium Planitia: Constraints for the InSight mission (expanded abstract) : 45<sup>th</sup> Lunar and Planetary Science, Abstract #2217, Lunar and Planetary Institute, Houston.
- Warner, N.H., et al., this issue, Near surface stratigraphy and regolith production in southwestern Elysium Planitia, Mars: Implications for Hesperian-Amazonian terrains and the InSight lander mission, *Space Science Reviews*, in review.

- Wigton, N. R., Warner, N., and Golombek, M., 2014, Terrain mapping of the InSight landing region: Western Elysium Planitia, Mars (expanded abstract) : 45<sup>th</sup> Lunar and Planetary Science, Abstract #1234, Lunar and Planetary Institute, Houston.
- Wood, D. M. (2003). *Geotechnical modelling* (Vol. 1). CRC Press.